Journal of ELECTRONIC MATERIALS, Vol. 48, No. 10, 2019
https://doi.org/10.1007/s11664-019-07319-y
© 2019 The Minerals, Metals & Materials Society

U.S. WORKSHOP ON PHYSICS AND CHEMISTRY OF II-VI MATERIALS 2018

# Carrier Transport in the Valence Band of nBn III–V Superlattice Infrared Detectors

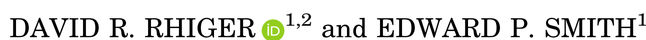

DAVID R. RHIGER[1,2] and EDWARD P. SMITH[1]

1.—Raytheon Vision Systems, Goleta, CA 93117, USA. 2.—e-mail: drhiger@raytheon.com

Mid-wavelength infrared detectors have been fabricated in the nBn configuration using the InAs/InAsSb superlattice as the absorber. Possible impediments in the valence band can interfere with the transport of holes that represent the signal. We demonstrate that the thermal activation energy of the photocurrent density, as a function of the applied bias voltage, can be a very sensitive probe of the valence band features. We identify and measure two types of impediments, the hole-block due to a band misalignment and the localization sites formed by fluctuations in the superlattice layer thicknesses. The latter are found to dominate the temperature dependence of the hole mobility. Our inferred localization characteristics are consistent with published results obtained by other techniques.

**Key words:** III–V superlattice, nBn, carrier transport, mobility, localization

## INTRODUCTION

Significant progress has been demonstrated recently in the development of infrared sensors based on III–V superlattice materials.[1–4] The most common device architecture is nBn, in which an *n*-type absorber and an *n*-type collector are separated by a unipolar conduction band barrier B. Infrared photons generate electron–hole pairs in the absorber, and the holes, moving in the valence band, must travel past the barrier to arrive at the collector. In this paper we address the issue of impediments to the transport of holes. Such impediments directly impact the quantum efficiency of the detector, and indirectly lead to an increase in the dark current because of the additional bias voltage that can be required to overcome an impediment.

Our experimental data are obtained with nBn devices having an absorber composed of the InAs/InAsSb superlattice with a mid-wave infrared (MWIR) cutoff between 5 $\mu$m and 6 $\mu$m. We describe a method for measuring the energy heights of the impediments in the valence band and apply it to several cases. Two types of impediments are identified. The first, which we call a hole-block, is a misalignment of the valence band at or near the absorber–barrier interface. The second type, known as localization sites, are distributed throughout the volume of the absorber and reduce the rate of diffusion of holes by capturing and releasing them at a thermally determined rate. We show examples of various types of hole-blocks, as well as some ideal cases having no hole-block. In addition, we present measurements of the energetic depth of the localization sites and obtain an estimate of their effect on the minority carrier mobility.

In nBn devices, valence band misalignments have been observed in several material systems. With an InAs/GaSb superlattice absorber, Rodriguez et al.[5] reported a hole-block requiring -300 mV bias to turn the device on fully (with no hole-block the turn-on can occur at zero bias). Lin et al.[6] using an InAsSb alloy absorber found a hole-block that needed $-$ 400 mV for full turn-on. Zuo et al.[7] identified a hole-block with an InAs/InAsSb superlattice absorber. Also, with the InAs/InAsSb superlattice, Ting et al. have made several observations of the hole-block effect[8–10] and they have modeled the bias dependence of the dark current[11] with the height of the hole-block as a parameter. Hole-blocks have also been identified in HgCdTe nBn structures.[12–14]

(Received April 2, 2019; accepted May 21, 2019;
published online June 3, 2019)

Evidence for localization sites has been reported by Steenbergen et al.[15] based on temperature-dependent photoluminescence, finding an average depth of about 8 meV for the sites in MWIR InAs/InAsSb superlattice samples. Further study of the localization phenomenon, in long wavelength infrared (LWIR) InAs/InAsSb, has been reported by Olson et al.[16] in terms of the temperature dependence of the hole mobility in the growth direction. Our results, obtained from the temperature dependence of the MWIR nBn photocurrent, are consistent with theirs.

## DEVICE FEATURES AND MANIFESTATION OF THE HOLE-BLOCK

Figure 1 is a qualitative sketch of the band profile of the nBn device when biased for normal operation. Both the absorber and collector are *n*-type. The barrier has a large bandgap extending into the conduction band to minimize dark current by blocking the flow of majority electrons. The substrate (not shown) is to the left and a metal contact (not shown) is on the right at the top of the device. Photoexcitation within the absorber produces minority holes that diffuse toward the barrier. The Fermi level in this illustration has been offset between the two sides by the negative bias voltage *V* applied to the metal contact. A hole-block, in this example, is present at the absorber-barrier interface, but holes are able to drift easily to the collector because the hole-block has been pulled up higher (lower energy for holes) than the valence band edge in the quasi-neutral region of the absorber. In this condition the hole-block does not diminish the quantum efficiency (QE). However, an undesirable consequence of the bias is an expansion of the depletion region in the absorber adjacent to the barrier, allowing the Shockley–Read–Hall (SRH) mechanism[17,18] to generate increased dark current.

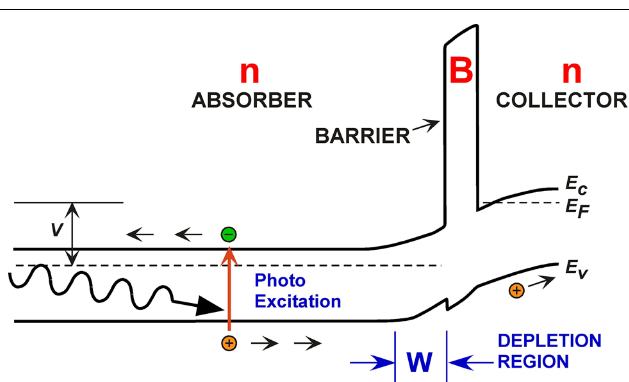


Fig. 1. Qualitative sketch of the band profile of the nBn device. Both the absorber and collector are *n*-type. The conduction and valence band edges are $E_c$ and $E_v$, respectively. The unipolar barrier blocks the flow of majority-carrier electrons. Infrared photons enter through the substrate (not shown) on the left and generate electron–hole pairs in the absorber. Holes move in the valence band to the collector. A small hole-block is illustrated at the absorber-barrier interface. A metal contact (not shown) at the top of the collector on the right applies a negative bias voltage, causing the offset in the Fermi level $E_F$.

The experimentally obtained spectral response curves in Fig. 2, acquired at a series of bias values, show the effect of a hole-block. The absorber and collector are InAs/InAsSb superlattices with an absorber thickness of 3.60 $\mu$m, and the barrier is an AlGaSbAs alloy 0.15 $\mu$m thick. This diode belongs to a mini-array with a 61-$\mu$m pitch and no antireflection coating. At zero bias QE is very small at all wavelengths, but it rises as the increasing bias overcomes the hole-block. The response begins to saturate when bias is more negative than approximately − 200 mV. To a very good approximation, all of the curves in Fig. 2 have the same shape, being related to one another by simple scaling. (The general invariance of the spectral shape with respect to bias is seen in many other samples.) Thus, a change in bias affects only the amplitude of the spectral response and not its wavelength dependence. We conclude that a change in bias does not modify the rate at which holes can diffuse through the quasi-neutral region, which occupies most of the volume of the absorber, to reach the edge of the depletion region, but it does control the rate at which holes move past the barrier to reach the collector.

An independent demonstration of the hole-block effect in the same sample can be obtained with the photocurrent density. We measure current versus bias under illumination from a 300 K blackbody with an *f*/2 field of view (FOV) and subtract the dark current measured in zero field of view (in radiative equilibrium with its cold surroundings). The photocurrent density is

$$J_{\text{photo}} = J_{\text{total}}(f/2, 300\text{KBB}) - J_{\text{dark}}(\text{FOV} = 0) \quad (1)$$

The result is the smooth curve in Fig. 3. The diamonds in this figure represent the spectral

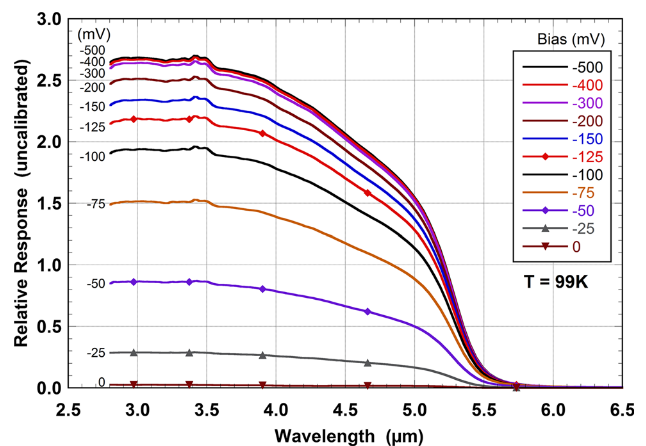


Fig. 2. Spectral response curves showing the dependence of the signal on the applied bias. This device has a hole-block, which is gradually overcome by the increasingly negative bias. Sample 688543-D9.

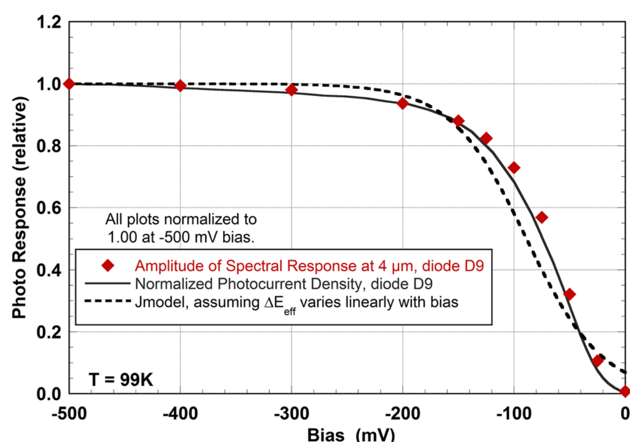


Fig. 3. Normalized response as a function of reverse bias for the same sample as Fig. 2. Diamond symbols are the amplitudes of the spectral response curves at 4 $\mu$m wavelength. The solid curve is the photocurrent density as defined in the text. The dashed curve is a calculation from a simplified thermionic emission model. Sample 688543-D9.

response amplitudes at a fixed wavelength of 4 $\mu$m taken from Fig. 2. Both plots have been normalized to 1.00 at $-$ 500 mV and show excellent agreement. The dashed curve in Fig. 3 is the fit of a model as explained below.

Test structure chips for this investigation were fabricated by standard photolithographic methods on wafers grown by molecular beam epitaxy with unintentional $n$-type doping of the absorber. In most cases the absorber thickness is between 3.5 $\mu$m and 4.0 $\mu$m. Each chip provides several mini-arrays and a set of variable area diodes. A chip is hybridized to a fanout board by means of indium bumps and mounted in a leadless chip carrier, forming a test structure assembly (TSA). Illumination is through the back side (substrate) in the same manner as a focal plane array. Additional details have been given elsewhere.[19] We refer to each sensing element as a diode because it is a two-terminal device, and each device is a mesa. Our sign convention refers to the polarity of the voltage $V$ applied to the top of the mesa.

## CHARACTERIZATION OF THE HOLE-BLOCK AND LOCALIZATION

Three conceptual illustrations of hole-blocks appear in Fig. 4. The first (a) is a misalignment of the bottom of the barrier. The second (b) is a band-bending misalignment at the interface, which could be caused, for example, by electron accumulation or increased doping at that location. The third (c) occurs between the barrier and collector, in which the conduction bands in the absorber and collector are approximately aligned due to their $n$-type doping, while the greater bandgap of the collector causes its valence band to introduce a step down. The fourth (d) item is a case of no hole-block, having good absorber-barrier alignment and a collector that offers no impediment to hole transport. It is

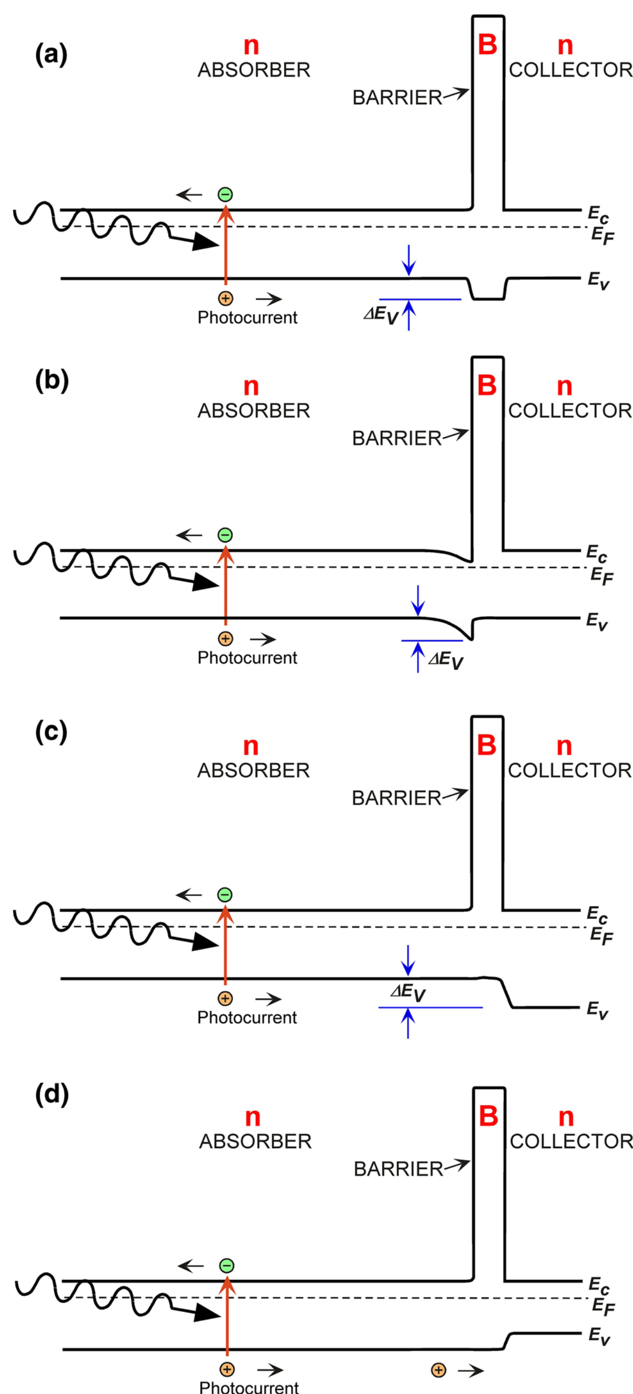


Fig. 4. Qualitative sketches of the band profiles with a variety of hole-block conditions. (a) Misalignment at the bottom of the unipolar barrier; (b) band-bending misalignment; (c) wider bandgap in the collector; (d) absence of a hole-block.

expected that the first two can be corrected by adjusting the composition or strain and the doping of the barrier or absorber material, and the third by reducing the collector bandgap. Other forms of hole-block can also be envisioned. Considering the example in Fig. 2, the absorber and collector were grown with the same bandgap and the same uniform

doping, making it very likely that in this case the hole-block can be correctly described by Fig. 4(a).

Each case in Fig. 4 is shown at zero bias (flat Fermi level) with the size of the hole-block, if present, defined as $\Delta E_v$. When the applied reverse bias is being increased, it pulls the bands upward at the location of the hole-block (as in Fig. 1), causing a diminishing effective step of magnitude $\Delta E_{eff}$ which will obey

$$\Delta E_v \geq \Delta E_{eff}(V) \geq 0 \qquad (2)$$

and after reaching sufficient negative bias $\Delta E_{eff}$ will go to zero and remain zero. The latter situation is represented in Fig. 1. We have developed a method for measuring the effective size $\Delta E_{eff}$ of the hole-block as a function of bias based on the thermal activation of carriers over the step. The actual height $\Delta E_v$ is then the value of $\Delta E_{eff}$ as bias approaches zero.

Initially we considered using the thermal activation energy of the dark current to measure $\Delta E_{eff}$. This approach has been used by Sidor et al.[20] In this process, thermal excitation across the gap in the absorber provides the supply of holes, after which they are available for thermal activation over the hole-block. This involves two excitation rates in series, each with its own Boltzmann factor $\exp(-E/kT)$, where $E$ is the characteristic energy, $k$ is Boltzmann's constant, and $T$ is the temperature. The experimentally measured quantity will be the sum of the activation energies. The measured thermal activation energy would then be given by

$$E_a(V) = (1-z)(E_g + 3kT) + z(E_g/2 + 3kT/2) + \Delta E_{eff}(V) + E_{loc} \qquad (3)$$

where $z$ represents the fraction of the hole population generated by the SRH mechanism in the depletion region and $E_g$ is the bandgap in the absorber, and the other fraction $(1-z)$ represents diffusion from the quasi-neutral region.[19] The $kT$ terms originate in the temperature dependence of the intrinsic carrier concentration $n_i$. The last term $E_{loc}$ is the localization energy, which is presumed to be bias independent, as discussed below. Since $z$ is not easily determined and it varies with bias, and because $\Delta E_{eff} + E_{loc}$ would be a minor part of the measured energy, we chose not to use this method.

Our preferred method is to use photo-excitation to supply the holes, a process that is nearly independent of temperature. Generation of holes is accomplished by exposure to 300 K blackbody flux at *f*/2 FOV, with photocurrent defined in Eq. 1. The hole-block itself, when present, becomes the feature that dominates the temperature dependence of the current, giving the activation energy

$$E_a(V) = \Delta E_{eff}(V) + E_{loc} + E_{\Delta g} \qquad (4)$$

This method introduces a small additional term $E_{\Delta g} = 2$ meV to account for the temperature dependence of the bandgap of the absorber, as evaluated below. Another advantage of using photo-excitation to supply the carriers is that the photocurrent can exceed the dark current by a factor between 2 and 1000 or more, depending on bias and other conditions, giving a stronger signal than with dark current alone. However, it does not drive the detector out of the low injection regime. The photo-generated minority carrier density $p_\Phi$ in steady state with zero current can be estimated by using the continuity equations[21,22] to obtain

$$p_\Phi \approx \alpha \Phi \tau \qquad (5)$$

where, for example, $\alpha = 2000\ \text{cm}^{-1}$ for the absorption coefficient, $\tau = 10^{-6}$ s for the minority carrier lifetime, and $\Phi = 7 \times 10^{14}\ \text{cm}^{-2}\ \text{s}^{-1}$ for the incident photon flux between 2.0 $\mu$m and 5.5 $\mu$m wavelength, giving $p_\Phi \approx 1.4 \times 10^{12}\ \text{cm}^{-3}$. This is a low-injection condition, being large compared to the equilibrium hole density at $T = 90$ K of about $10^6\ \text{cm}^{-3}$, but small compared with the majority electron density, typically $4 \times 10^{15}\ \text{cm}^{-3}$.

The small $E_{\Delta g}$ term in Eq. 4 accounts for the increasing cutoff wavelength as temperature rises. It has been evaluated using the device in Fig. 2. Between 78 K and 103 K we measured $dE_g/dT = -1.56 \times 10^{-4}$ eV/K, which lengthens the cutoff from 5.23 $\mu$m at 78 K to 5.32 $\mu$m at 103 K. The approach is to calculate the absorbed blackbody flux as follows, and to approximate it as a thermally activated quantity:

$$\int_{4.5\ \mu\text{m}}^{6.0\mu\text{m}} \Phi(\lambda) R(\lambda, T) d\lambda \approx C \exp\left(-\frac{E_{\Delta g}}{kT}\right) \qquad (6)$$

where $C$ is a constant, and $\Phi(\lambda)$ is the cumulative incident flux[23] (photons $\text{cm}^{-2}\ \text{s}^{-1}$) from 3.3 $\mu$m up to the wavelength $\lambda$, which is the variable of integration. The contribution is negligible when shorter than 3.3 $\mu$m. The limits of integration cover the spectral range that is sensitive to the detector cutoff. $R(\lambda, T)$ is the experimental spectral response curve. The left-hand side of Eq. 6 was evaluated using spectral responses at 78 K, 90 K, and 103 K, and the results were analyzed by the Arrhenius method, obtaining $E_{\Delta g} = 2$ meV.

To summarize, the measured thermal activation energy of the photocurrent density will have three contributions according to Eq. 4. We apply the method to the sample shown in Fig. 2. The photocurrent density, defined by Eq. 1, is shown at several temperatures in Fig. 5. At each bias voltage we perform the Arrhenius analysis of the photocurrent and obtain the thermal activation energy presented also in Fig. 5. As bias becomes more negative, $E_a(V)$ falls until the bias goes just beyond -200 mV, consistent with Figs. 2 and 3, and then reaches a bias-independent value of about 7 meV. The latter is assigned to $E_{loc} + E_{\Delta g}$, giving $E_{loc} = 5$ meV. The projection to zero bias is

35 meV, indicating that the size of the hole-block is $\Delta E_v \approx 28$ meV.

## SIMPLIFIED THERMIONIC EMISSION MODEL

We present a simplified model to represent both the increase and the saturation of the minority-hole photocurrent thermally excited over the hole-block while the effective size $\Delta E_{\mathrm{eff}}$ of the hole-block is being diminished due to the reverse bias. The principal source of holes is assumed to be photogeneration in the absorber. We adapt the basic equation for thermionic emission of electrons.[17]

$$J_{\mathrm{thermionic}} = qnv \exp\left(\frac{-\Delta E_{\mathrm{eff}}}{kT}\right) \qquad v = \sqrt{\frac{kT}{2\pi m^*}} \quad (7)$$

where $n$ is the electron density, $q$ is the unit charge, and $v$ is the velocity dependent on the effective mass $m^*$. In the case of electrons emitted by an $n$-type semiconductor into a metal, as in a Schottky barrier, the electron density $n$ would be expressed in terms of the Fermi level and the conduction band density of states, leading to the familiar Schottky current equation.[24] The current would increase exponentially with bias, fed by the nearly unlimited supply of majority carriers. In contrast, in the nBn detector, the minority current passing over the hole-block will reach a saturation level. Because it operates in low level photo-injection, there will be a limited population of minority carrier holes determined by the photon flux. The hole density $p$ in the absorber will decrease as the current density flowing out of the absorber increases. For simplicity we assume a uniform photo-generation rate $G$, a carrier lifetime $\tau$, and a hole diffusion length $L$. Using the standard drift–diffusion and continuity equations[21,22] we find $p = G\tau - (\tau/qL)J_{\mathrm{thermionic}}$. We insert this $p$ in place of $n$ in Eq. 7 and solve for $J_{\mathrm{thermionic}}$ to obtain

$$J_{\mathrm{thermionic}} = \frac{G\tau qv \exp(-\Delta E_{\mathrm{eff}}/kT)}{1 + \frac{\tau v}{L}\exp(-\Delta E_{\mathrm{eff}}/kT)} \quad (8)$$

A further assumption to facilitate this model is that the decrease of $\Delta E_{\mathrm{eff}}$ with bias is a linear function. Equation 8 gives the dashed curve in Fig. 3 when we take $T$ = 99 K, $\Delta E_v$ = 90 meV, $\mathrm{d}\Delta E_{\mathrm{eff}}/\mathrm{d}V$ = 0.25 eV/V, $\tau$ = 0.5 $\mu$s, $L$ = 5 $\mu$m, and $m^*$ = 0.3 $m_0$, where $m_0$ is the free electron mass. These values constitute a non-unique set that gives a reasonable fit. However, they are not a quantitatively accurate representation of the actual device because of the simplifying assumptions of the model. The usefulness of the model is that it conceptually illustrates, first, the control of the photocurrent by thermionic emission over the bias-dependent hole-block, and second, the saturation of the photocurrent at large reverse bias due to the limited supply of holes.

## ADDITIONAL EXAMPLES

In another example, the nearly complete absence of a hole-block is indicated by the spectral response curves in Fig. 6, which show very little change with bias. The amplitudes of these curves at 4 $\mu$m wavelength are plotted versus bias with the diamond symbols in Fig. 7. The upper smooth curve in Fig. 7 is the normalized photocurrent density. These two independent measurements track well together. The presence of an almost negligible hole-block is suggested by the thermal activation energy of the photocurrent, which is the lower curve in Fig. 7, showing a very small rise in the approach to zero bias, but beyond − 50 mV a nearly constant sum $E_{\mathrm{loc}} + E_{\Delta g}$ of about 8 meV, implying $E_{\mathrm{loc}}$ = 6 meV.

We have defined the combination $E_{\mathrm{loc}} + E_{\Delta g}$ as the bias-independent component of the thermal activation energy of the photocurrent that appears at sufficient negative bias. Several examples for MWIR InAs/InAsSb nBn detectors are shown in Fig. 8.

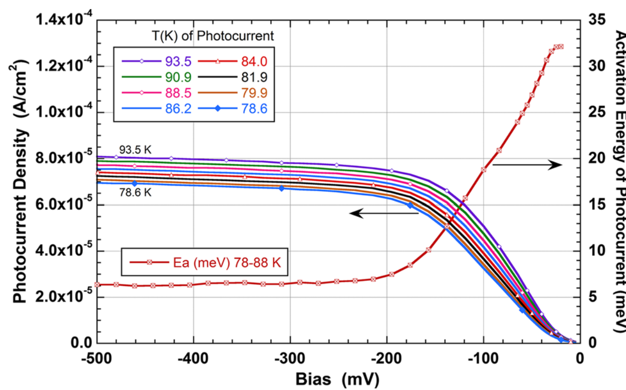


Fig. 5. Application of the photocurrent thermal activation energy technique to the sample in Fig. 2. Left axis is the photocurrent density at several temperatures. Right axis is the activation energy at each bias voltage obtained by Arrhenius analysis of the photocurrent. It projects to 35 meV at zero bias and levels off at about 7 meV at large bias. The hole-block is overcome at about -200 mV. Sample 688543-D9.

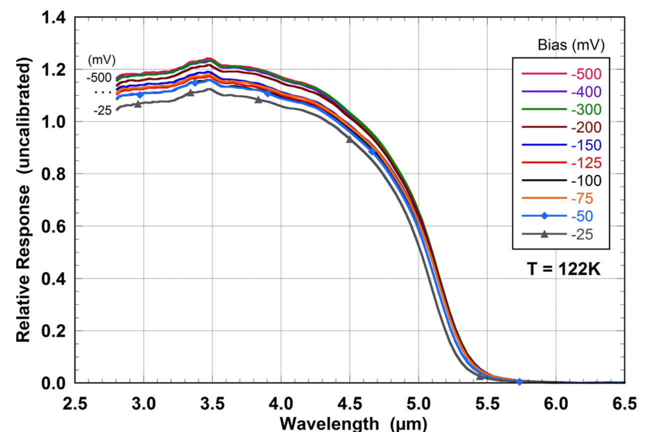


Fig. 6. Spectral response curves for a sample having almost no hole-block. Sample 688481-D15.

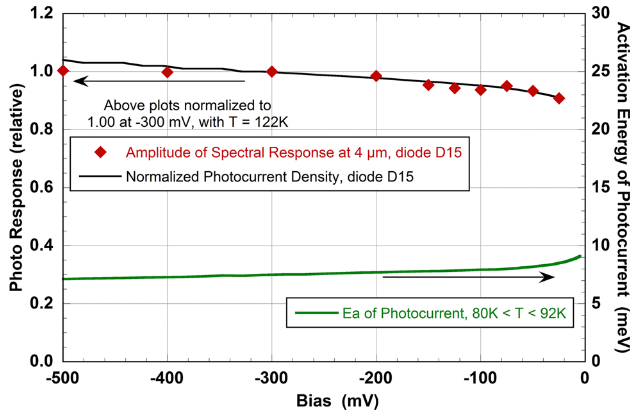


Fig. 7. Normalized response as a function of reverse bias for the same sample as Fig. 6. Diamond symbols are the amplitudes of the spectral response curves at 4 $\mu$m wavelength. The upper solid curve is the photocurrent density. Right axis: the lower solid curve is the thermal activation energy of the photocurrent. Sample 688481-D15.

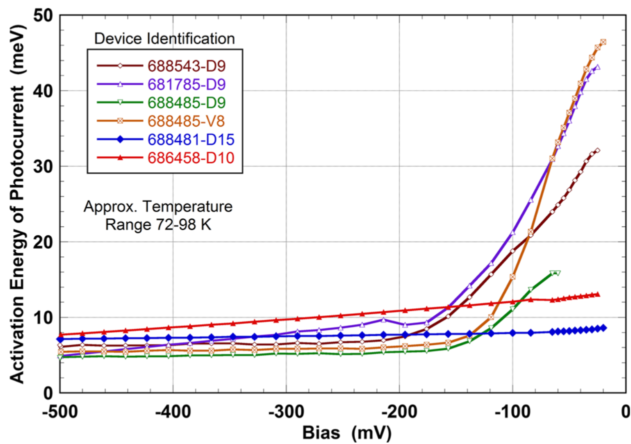


Fig. 8. Activation energy of the photocurrent versus bias, for six different InAs/InAsSb nBn samples. The greatest hole-block (by projecting to zero bias) is about 50 meV. At large bias all curves approximately level off between 5 meV and 9 meV, where the relative bias-independence indicates that the localization sites occur within the quasi-neutral region of the absorber, in which the applied bias does not produce an electric field.

Between 0 mV and − 200 mV many of them reveal a hole-block, with the largest projecting at zero bias to $\Delta E_v \approx$ 50 meV. However, when bias is more negative than − 200 mV the hole-blocks have been overcome and the residual $E_{\rm loc} + E_{\Delta g}$, mostly between 5 meV and 9 meV, is evident, giving $E_{\rm loc}$ approximately between 3 meV and 7 meV. The lack of any strong bias dependence suggests that the mechanism originates in the quasi-neutral region of the absorber, which does not experience the electric field of the applied bias voltage. (The depletion region is only about 0.5 $\mu$m thick compared with the absorber thickness of 3.9 $\mu$m, for example.) This is consistent with the presence of localization sites caused most likely by material nonuniformities that are distributed throughout the volume of the absorber.

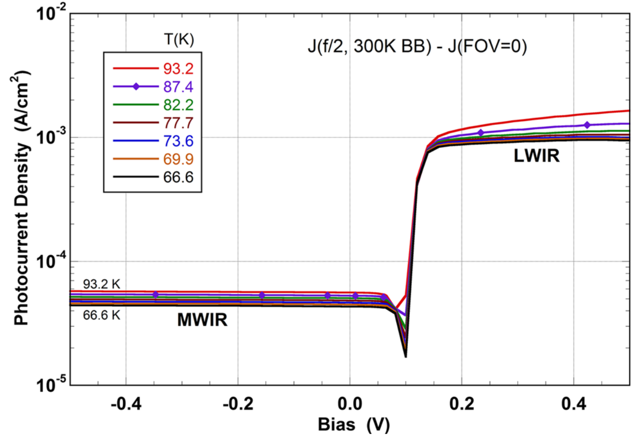


Fig. 9. Photocurrent density for a dual-band nBn InAs/InAsSb device, at several temperatures. The MW and LW response regimes are labeled. Sample 688481-D15.

For comparison we performed the same measurement of photocurrent versus temperature on a conventional planar InSb detector. It had been fabricated from a bulk-grown single-crystal $n$-type wafer with a $p$-type ion implant to form the $p$–$n$ junction. The absorber is 10 $\mu$m thick. In the 68 K to 86 K temperature range we found the thermal activation energy of the photocurrent $E_{\rm a}(V)$ to be uniformly 1 meV over the bias range 0 mV to − 700 mV. Also $dE_g/dT \approx -1.6 \times 10^{-4}$ eV/K for InSb[25] in this temperature range, similar to the superlattice, so again $E_{\Delta g} \approx$ 2 meV. Thus, within experimental uncertainty $E_{\rm loc}$ is indistinguishable from zero. Consequently, for the InSb detector it is clear that, first, there is no hole-block, and second, there is no evidence of carrier localization.

Hole-block effects can also be invoked to characterize the response of a dual-band MW/LW nBn device. Both $n$-type regions serve as absorbers and have similar thicknesses, with the MW absorber being closer to the substrate for back side illumination. For the example in Fig. 9, the MW photocurrent density remains independent of bias from − 500 mV almost up to + 100 mV, implying that there is no hole-block for holes flowing from the MW absorber into the LW absorber, which serves as the collector for the MW current. Apparently, the composition and doping of the MW absorber and unipolar barrier have been optimized for easy flow of the holes in MW operation. The decrease in bandgap going into the LW absorber is also favorable. When bias is greater than about + 130 mV, holes from the LW absorber flow in the other direction. The changeover from one band to the other occurs within a narrow interval of bias (+ 90 mV to + 130 mV), as shown by the spectral responses in Fig. 10. Band profiles are sketched qualitatively in Fig. 11. Bandgaps of the MW and LW absorbers are 243 meV and 122 meV, respectively, and they have the same $n$-type doping, so the difference appears in the valence band. Holes

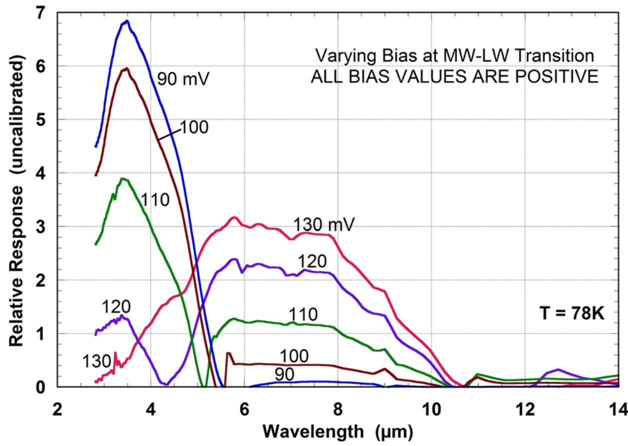


Fig. 10. Spectral response curves in the bias interval of + 90 mV to + 130 mV, for the same dual band sample in Fig. 9. The changeover from MW to LW response occurs in this narrow interval, determined by the difference in bandgap between the two absorbers. Bias during normal operation, for MW or LW, would be well outside of this interval. Sample 688481-D15.

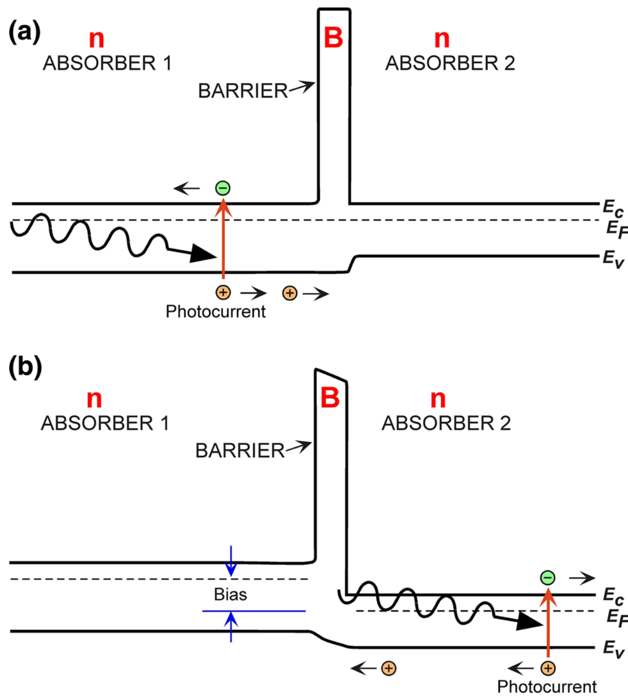


Fig. 11. Qualitative sketches of the band profiles for the dual-band device, (a) at zero bias, where MW response occurs, and (b) at positive bias for LW response. The valence band step between absorber 2 and the barrier is overcome when bias is sufficiently positive.

attempting to flow from the LW absorber encounter a hole-block until a sufficiently positive bias overcomes the valence band step. The bandgap difference, namely 121 meV, corresponds to the changeover bias interval in Fig. 10.

## LOCALIZATION EFFECT AND MOBILITY

We address the issue of hole transport in order to understand the mechanisms affecting quantum efficiency $\eta$. In particular, we show that the experimentally measured value of the localization energy $E_{\rm loc}$ enables us to obtain an estimate of the temperature dependence of the hole mobility. An important intermediate step involves the temperature dependence of the hole diffusion length $L_{\rm h}$ as explained below. This analysis applies to the single-color MWIR nBn detector.

First it is noted that we have assumed the photocurrent density to be thermally activated with the characteristic energy $E_{\rm a}$ given in Eq. 4, so that

$$J_{\rm photo} = J_{\rm photo0} \exp\left(-\frac{E_{\rm loc} + E_{\Delta g}}{kT}\right) \tag{9}$$

where $J_{\rm photo0}$ is a reference value. Here we have set $\Delta E_{\rm eff} = 0$ corresponding to a bias range in which a hole-block is not important. Then

$$\frac{1}{J_{\rm photo}} \frac{{\rm d}J_{photo}}{{\rm d}T} = \frac{E_{\rm loc}}{kT^2} + \frac{E_{\Delta g}}{kT^2} \tag{10}$$

The second term on the right represents the contribution originating at wavelengths near the changing cutoff. The first term embodies the other temperature-dependent effects. Now considering the quantum efficiency $\eta$, it will scale with temperature in a similar manner as the photocurrent, but with the exception that the $E_{\Delta g}$ term does not apply because it is typically measured with a narrow pass filter at a wavelength not close to the cutoff. Thus,

$$\frac{1}{\eta}\frac{{\rm d}\eta}{{\rm d}T} = \frac{E_{\rm loc}}{kT^2} \tag{11}$$

Taking 5 meV as the median value of $E_{loc}$ for the examples in Fig. 8 and their mid-range temperature of 85 K, we obtain $(1/\eta)({\rm d}\eta/{\rm d}T) = 8.03 \times 10^{-3}$ K$^{-1}$. This number is used below.

We are aiming to find the temperature dependence of the hole mobility by investigating the behavior of the hole diffusion length $L_h$, which is expressed as[17]

$$L_{\rm h} = \sqrt{D_{\rm h}\tau_{\rm h}} = \sqrt{\frac{k}{q}\tau_{\rm h}\mu_{\rm h}T} \tag{12}$$

where $D_{\rm h}$ is the hole diffusivity, $\tau_{\rm h}$ is the minority carrier lifetime, and $\mu_{\rm h}$ is the hole mobility. Allowing both lifetime and mobility to depend on temperature we find

$$\frac{{\rm d}L_{\rm h}}{{\rm d}T} = \frac{L_{\rm h}}{2}\left[\frac{1}{\tau_{\rm h}}\frac{{\rm d}\tau_{\rm h}}{{\rm d}T} + \frac{1}{\mu_{\rm h}}\frac{{\rm d}\mu_{\rm h}}{{\rm d}T} + \frac{1}{T}\right] \tag{13}$$

It has been shown experimentally by Aytac et al.[26,27] and by Olson et al.[28] (using methods that do not depend on mobility) that in multiple samples of $n$-type MWIR InAs/InAsSb superlattices the minority carrier lifetime is almost temperature-independent between 75 K and 175 K due to limitation by the SRH mechanism. Thus, we can neglect the lifetime term in Eq. 13, and therefore,

$$\frac{1}{\mu_h}\frac{d\mu_h}{dT} \approx \frac{2}{L_h}\frac{dL_h}{dT} - \frac{1}{T} \tag{14}$$

Additionally, the temperature dependence of QE can be related to the hole diffusion length as follows.

$$\frac{d\eta}{dT} = \frac{d\eta}{dL_h}\frac{dL_h}{dT} \tag{15}$$

from which

$$\frac{dL_h}{dT} = \frac{(1/\eta)(d\eta/dT)}{(1/\eta)(d\eta/dL_h)} \tag{16}$$

The numerator on the right was evaluated above. To find the denominator we calculate the dependence of $\eta$ on the diffusion length by means of the Hovel equations[24,29] which give QE as a function of several device parameters. Taking a typical example, assumptions are that the absorber thickness is 3.5 $\mu$m, $L_h$ = 4.0 $\mu$m, the absorption coefficient is 2000 $cm^{-1}$, that surface recombination is negligible, that negligible absorption occurs in the collector because it is thin, and that the photons have 0.6 reflectivity from the top metal to make a second pass. This combination gives $\eta$ = 0.52, assuming a perfect antireflection coating at the back side entrance surface. The relation between QE and diffusion length, however, is independent of the back side coating. The result is $(1/\eta)(d\eta/dL_h) = 0.1035\ \mu m^{-1}$.

Next, to get the temperature dependence of the mobility, we insert $dL_h/dT$ from Eq. 16 into Eq. 14 to obtain

$$\frac{1}{\mu_h}\frac{d\mu_h}{dT} = \frac{2}{L_h}\frac{(1/\eta)(d\eta/dT)}{(1/\eta)(d\eta/dL_h)} - \frac{1}{T} \tag{17}$$

As stated above we are using the median $E_{loc}$ (5 meV) and mid-range temperature (85 K) of the examples in Fig. 8, so that Eq. 17 evaluates to

$$\frac{1}{\mu_h}\frac{d\mu_h}{dT} = 0.039\,K^{-1} - 0.012\,K^{-1} = 0.027\,K^{-1} \tag{18}$$

for the temperature dependence of mobility. The first term (0.039 $K^{-1}$) originates with carrier localization and the second (0.012 $K^{-1}$) derives from the explicit temperature factor in the diffusion length in Eq. 12. The localization effect in this example is about three times larger than the explicit temperature contribution. (A supplementary result is that $dL_h/dT \approx$ 0.08 $\mu$m/K.) The material parameters assumed in the above estimate represent a typical InAs/InAsSb MWIR nBn detector, but they can vary from one case to another. Also, it should be recognized that these values apply within a limited temperature range of about 70 K to about 100 K. Nevertheless, it is clear that, in the absence of a hole-block, the temperature dependence of QE is dominated by the temperature dependence of the mobility.

## DISCUSSION OF LOCALIZATION

The hypothesis is that localization sites caused by material nonuniformities are distributed throughout the volume of the absorber, and that holes diffusing through the absorber are delayed by temporary capture in these sites. In the nBn device the localization sites influence the quantum efficiency through their effect on the hole mobility. The temperature dependence is due to thermal excitation of holes out of these sites into the extended-state HH1 valence band[4] in which they are mobile and able to diffuse.

There have been at least three investigations of the localization phenomenon in the InAs/InAsSb superlattice, each using a different experimental technique. The first, by Steenbergen et al.,[15] used temperature-dependent and excitation-dependent photoluminescence (PL) spectroscopy in MWIR samples to demonstrate the existence of the sites and to measure their energy depth. The second, by Olson et al.,[16] used the characteristics of a specially made bipolar heterojunction transistor with a base consisting of LWIR (12.5 $\mu$m cutoff) InAs/InAsSb to measure the hole mobility in the growth direction as a function of temperature. The third is the present work, in which we have used the temperature dependence of the photocurrent in MWIR nBn devices to measure the energy depth of the localization sites and demonstrate that they are distributed throughout the absorber volume.

The three investigations are mutually supportive. Steenbergen found a blue shift of 8 meV in the PL peak position with temperature, which is a measure of the depth of the average localization site. This falls within the range of $E_{loc}$ values we have found at negative bias (Fig. 8). With the PL technique,[15] however, the experimental manifestation of the localization sites occurred mainly for $T < 60$ K, whereas our photocurrent results were obtained for $T > 70$ K. We suggest that the sensitivity of our photocurrent technique in the higher temperature range is possible because of the lower level of injection ($\delta p \approx 10^{12}$ $cm^{-3}$) as compared with the elevated level ($\delta p \approx 10^{16}$ $cm^{-3}$) in the PL technique, keeping the localizations sites far from saturation. In the other investigation, Olson[16] found that the hole mobility exhibits different behavior in four separate temperature intervals. Their interval number 2 (67–110 K) best corresponds to the interval (72–98 K) of our results in Fig. 8. They reported an activation energy of 36 meV for the mobility $\mu_h$.

This differs from our 5 meV activation energy of the photocurrent, but it is not in conflict because in any practical device the photocurrent is not simply proportional to the mobility. Taking Olson's thermal activation energy, with 89 K as the mid-range temperature (of their interval 2) gives $(1/\mu_\mathrm{h})(\mathrm{d}\mu_\mathrm{h}/\mathrm{d}T) = (36\,\mathrm{meV})/(kT^2) = 0.053\,\mathrm{K}^{-1}$. This differs from our result in Eq. 18 by a factor of 2, which should be regarded as reasonable agreement, considering the approximations in our calculation, and that Olson's result was obtained from LWIR material.

The investigation of Yoon et al.[30] provides another example for comparison. By a modified technique of electron beam induced current they measured minority carrier vertical diffusion lengths in several nBn superlattice devices. The temperature dependence of their resulting hole mobility in MWIR InAs/InAsSb between 80 K and 160 K reveals a thermal activation energy of 27 meV, implying $(1/\mu_\mathrm{h})(\mathrm{d}\mu_\mathrm{h}/\mathrm{d}T) = 0.022\ \mathrm{K}^{-1}$, similar to our Eq. 18. The authors did not discuss the issue of localization.

Also, a comparison with our InSb result is instructive. Being a bulk-grown binary compound, this sample is free of any internal interfaces and any alloy disorder. Accordingly, the thermal activation energy of the photocurrent shows no evidence of either a hole-block or the localization sites. A further clue is available from Lin et al.,[31] who found by PL that a 1-$\mu$m-thick single-layer sample of InAsSb alloy showed no evidence of localization sites. Both results support the idea that the localization sites are caused by spatial fluctuations in the superlattice layer thicknesses, or the InAsSb composition within the superlattice layers.

## SUMMARY

We have measured and analyzed the temperature dependence of the photo-generated current density in MWIR InAs/InAsSb superlattice nBn devices, and have demonstrated that this technique is a sensitive probe of hole transport. Treating the photocurrent as a thermally activated quantity, we have obtained its thermal activation energy as a function of bias voltage. This reveals, and quantifies, two types of impediments to hole transport. The first is the hole-block features due to misalignments at the absorber-barrier interface and possibly the barrier-collector interface, and the second is the localization sites within the quasi-neutral region of the absorber. We have found a case of hole-block as large as 50 meV and other cases where it is nonexistent, and have given plausible explanations in terms of the band profiles. The effective height of the hole-block can be diminished by increasing the bias voltage, but at the cost of adding to the SRH dark current.

Regarding the localization sites, our measurements show their typical depth (for hole capture) $E_\mathrm{loc}$ to be approximately 5 meV. Also, the bias independence of the activation energy, when the hole-block is not participating, demonstrates that these sites are distributed throughout the volume of the absorber, as would be expected for features originating in the superlattice growth process. The absence of localization sites in non-superlattice samples indicates that they arise from nonuniformities associated with the superlattice layers, most likely fluctuations in thickness.

## ACKNOWLEDGMENTS

Work supported by M. Tidrow and S. Bandara of U.S. Army Night Vision and Electronic Sensors Directorate (NVESD), Contract W15P7T-06-D-E402. Wafers were grown by IQE and Intelligent Epitaxy. The authors acknowledge helpful discussions with S.M. Johnson, J.I. Mustafa, and C.A. Keasler of Raytheon and D.Z. Ting of Jet Propulsion Laboratory. Device testing was performed by J. Choquette-Ortega.

## CONFLICT OF INTEREST

The authors declare they have no conflict of interest.

## REFERENCES


1. A. Rogalski, M. Kopytko, and P. Martyniuk, *Antimonide-Based Infrared Detectors A New Perspective* (Bellingham: SPIE Press, 2018).
2. M. Razeghi, A. Haddadi, A. Dehzangi, R. Chevallier, and T. Yang, *Proc. SPIE* 10177, 1017705 (2017).
3. P. Martyniuk, M. Kopytko, and A. Rogalski, *Opto-Electron. Rev.* 22, 127 (2014).
4. D.Z.-Y. Ting, A. Soibel, L. Höglund, J. Nguyen, C.J. Hill, A. Khoshakhlagh, and S.D. Gunapala, Type – II superlattice infrared detectors.*Semiconductors and Semimetals*, Vol. 84, ed. S.D. Gunapala, D.R. Rhiger, and C. Jagadish (Amsterdam: Elsevier, 2011), pp. 1–57.
5. J.B. Rodriguez, E. Plis, G. Bishop, Y.D. Sharma, H. Kim, L.R. Dawson, and S. Krishna, *Appl. Phys. Lett.* 91, 043514 (2007).
6. Y. Lin, D. Wang, D. Donetsky, G. Kipshidze, L. Shterengas, L.E. Vorobjev, and G. Belenky, *Semicond. Sci. Technol.* 29, 112002 (2014).
7. D. Zuo, R. Liu, D. Wasserman, J. Mabon, Z.Y. He, S. Liu, Y.H. Zhang, E.A. Kadlec, B.V. Olson, and E.A. Shaner, *Appl. Phys. Lett.* 106, 071107 (2015).
8. D.Z. Ting, A. Soibel, L. Hoglund, C.J. Hill, S.A. Keo, A. Fisher, and S.D. Gunapala, *J. Electron. Mater.* 45, 4680 (2016).
9. A. Soibel, C.J. Hill, S.A. Keo, L. Hoglund, R. Rosenberg, R. Kowalczyk, A. Khoshakhlagh, A. Fisher, D.Z. Ting, and S.D. Gunapala, *Appl. Phys. Lett.* 105, 023512 (2014).
10. D.Z. Ting, A. Soibel, A. Khoshakhlagh, S.B. Rafol, S.A. Keo, L. Hoglund, A.M. Fisher, E.M. Luong, and S.D. Gunapala, *Appl. Phys. Lett.* 113, 021101 (2018).
11. D.Z. Ting, A. Soibel, L. Hoglund, and S.D. Gunapala, *J. Electron. Mater.* 44, 3036 (2015).
12. N.D. Akhavan, G. Jolley, G.A. Umana-Membreno, J. Antoszewski, and L. Faraone, *IEEE Trans. Electron Dev.* 62, 722 (2015).
13. M. Kopytko, J. Wrobel, K. Jozwikowski, A. Rogalski, J. Antoszewski, N.D. Akhavan, G.A. Umana-Membreno, L. Faraone, and C.R. Becker, *J. Electron. Mater.* 44, 158 (2015).

14. M. Koptyko, K. Jozwikowski, P. Martyniuk, W. Gawron, P. Madejczyk, A. Kowalewski, O. Markowska, A. Rogalski, and J. Rutkowski, *J. Electron. Mater.* 45, 4563 (2016).
15. E.H. Steenbergen, J.A. Massengale, G. Ariywansa, and Y.H. Zhang, *J. Lumin.* 178, 451 (2016).
16. B.V. Olson, J.F. Klem, E.A. Kadlec, J.K. Kim, M.D. Goldflam, S.D. Hawkins, A. Tauke-Pedretti, W.T. Coon, T.R. Fortune, E.A. Shaner, and M.E. Flatte, *Phys. Rev. Appl.* 7, 024016 (2017).
17. M.A. Kinch, *State-of-the-Art Infrared Detector Technology* (SPIE Press, Bellingham, 2014), pp. 44, 58, 134.
18. A.S. Grove, *Physics and Technology of Semiconductor Devices* (New York: Wiley, 1967), p. 129.
19. D.R. Rhiger, E.P. Smith, B.P. Kolasa, J.K. Kim, J.F. Klem, and S.D. Hawkins, *J. Electron. Mater.* 45, 4646 (2016).
20. D.E. Sidor, G.R. Savich, X. Du, and G.W. Wicks, *Infrared Phys. Technol.* 70, 111 (2015).
21. S.L. Chuang, *Physics of Photonic Devices*, 2nd ed. (Hoboken: Wiley, 2009), p. 32.
22. A. Rogalski, A. Jozwikowska, K. Jozwikowski, and J. Rutkowski, *Infrared Phys.* 33, 463 (1992).
23. A. Rogalski, *Infrared Detectors* (Boca Raton: CRC Press, 2011), p. 10.
24. A. Rogalski, K. Adamiec, and J. Rutkowski, *Narrow-Gap Semiconductor Photodiodes* (SPIE Optical Engineering Press, Bellingham, 2000), pp. 134, 154.
25. P.W. Kruse, Indium antimonide photoconductive and photoelectromagnetic detectors.*Semiconductors and Semimetals*, Vol. 5, ed. R.K. Willardson and A.C. Beer (New York: Academic Press, 1970), pp. 15–83.
26. Y. Atac, B.V. Olson, J.K. Kim, E.A. Shaner, S.D. Hawkins, J.F. Klem, M.E. Flatte, and T.F. Boggess, *J. Appl. Phys.* 118, 125701 (2015).
27. Y. Atac, B.V. Olson, J.K. Kim, E.A. Shaner, S.D. Hawkins, J.F. Klem, M.E. Flatte, and T.F. Boggess, *Proc. SPIE* 9370, 93700 J (2015).
28. B.V. Olson, E.A. Kadlec, J.K. Kim, J.F. Klem, S.D. Hawkins, and E.A. Shaner, *Phys. Rev. Appl.* 3, 044010 (2015).
29. H.J. Hovel, Solar cells.*Semiconductors and Semimetals*, Vol. 11, ed. R.K. Willardson and A.C. Beer (New York: Academic Press, 1975), .
30. N. Yoon, C.J. Reyner, G. Ariyawansa, J.M. Duran, J.E. Scheihing, J. Mabon, and D. Wasserman, *J. Appl. Phys.* 122, 074503 (2017).
31. Z.Y. Lin, S. Liu, E.H. Steenbergen, and Y.H. Zhang, *Appl. Phys. Lett.* 107, 201107 (2015).

**Publisher's Note** Springer Nature remains neutral with regard to jurisdictional claims in published maps and institutional affiliations.